I. SCHINDLER©[1*], P. KAWULOK©[1], K. KONEČNÁ©[1], M. SAUER©[1],
H. NAVRÁTIL©[1], P. OPĚLA©[1], R. KAWULOK©[1], S. RUSZ©[1]

SIMULATION OF HOT CONTINUOUS ROLLING OF A PLAIN CARBON STEEL USING
THE MAXSTRAIN II® MULTI-AXIS DEFORMATION SYSTEM

A simple methodology was used for calculating the equivalent strain values during forming the sample alternately in two mutually perpendicular directions. This method reflects an unexpected material flow out of the nominal deformation zone when forming on the MAXStrain II device. Thus it was possible to perform two temperature variants of the simulation of continuous rolling and cooling of a long product made of steel containing 0.17% C and 0.80% Mn. Increasing the finishing temperature from 900°C to 950°C and decreasing the cooling rate from 10°C/s to 5°C/s led to a decrease in the content of acicular ferrite and bainite and an increase in the mean grain size of proeutectoid ferrite from about 8 μm to 14 μm. The result was a change in the hardness of the material by 15%.

Keywords: MAXStrain II system; multi-axis deformations; hot continuous rolling; physical simulation

1. Introduction

Physical simulations are a highly effective tool for optimizing bulk-forming and controlled cooling processes of various metallic materials. Specialized deformation simulators allow precise control and a wide range of operational changes of individual temperature and deformation parameters of tests depending on time. The servo-hydraulic hot deformation simulator Gleeble 3800-GTC at VŠB – Technical University of Ostrava uses interrupted anisothermal compression tests of various types in simulations [1,2]. The uniaxial compression test (Fig. 1) is the most suitable for simulating upsetting operations. The samples (usually 10 mm in diameter and 15 mm high) can be resistively heated in a vacuum chamber to a temperature of up to 1700°C and formed with a maximum force of 196 kN. During each pass, the Hydrawedge II® Mobile Conversion Unit (MCU) ensures a nearly constant strain rate in the range of 0.001-100 s^{-1}.

The Plain Strain Compression Test (PSCT) is particularly suitable for simulating the rolling processes and selected forging operations. The samples are deformed most often from an initial height of 10 mm by anvils narrower than the initial width of the specimen (Fig. 2). The loose ends of the sample then prevent the material from spreading. Up to 20 passes can be programmed per test, depending on time, corresponding to differ-
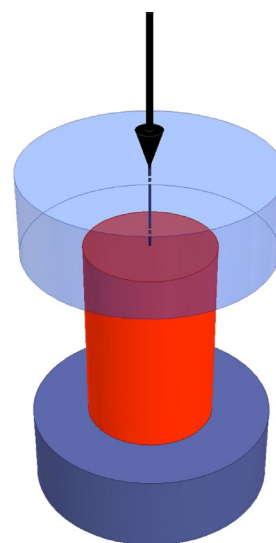

Fig. 1. Uniaxial compression test scheme (heated sample marked in red)

ent temperature, strain and strain rate (nominally max. 100 s^{-1}), with individual interpass times of less than 0.2 s. Thanks to thermocouples welded to the side of the deformation zone, PSCT allows relatively the most precise control of the rapid temperature changes during the forming and final cooling of the sample [3].

[1] VŠB – TECHNICAL UNIVERSITY OF OSTRAVA, FACULTY OF MATERIALS SCIENCE AND TECHNOLOGY, OSTRAVA, CZECH REPUBLIC

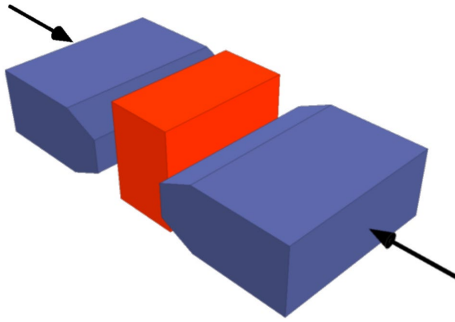* Corresponding author: ivo.schindler@vsb.cz

Fig. 2. Hot PSCT scheme

However, both tests described above have one significant shortcoming, related to the limited ability to achieve large cumulative strains. For example, if we needed to simulate the rolling of a 6 mm diameter bar from a 155 mm square billet, we would have to simulate an elongation of approximately 76.4×. This would mean a reduction in height to a finite 0.2 mm when upsetting a 15 mm high specimen (uniaxial pressure), which is practically infeasible. Even with PSCT, the final height of the deformed part of the sample is realistically only about 1 mm. It is possible to work with slightly larger initial dimensions of sample, but these do not allow sufficiently precise control of the rapid temperature changes, especially in the cooling phase of the investigated material.

This fundamental problem should be solved by alternating the deformation of a part of the sample in two directions when the sample is rotated along its longitudinal axis by 90° during the interpass times – see Fig. 3.
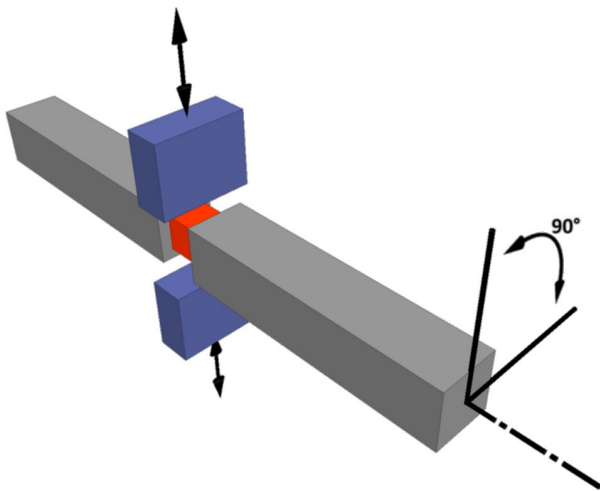

Fig. 3. Test scheme with alternating compressive deformations on the MCU MAXStrain II (deformation zone of the sample marked in red)

The MCU MAXStrain II allows programming of up to 80 defined passes with the shortest interpass times of about 0.7 s. Resistance heating (at up to 50°C/s in the case of steel) is controlled by thermocouple readings, obliquely drilled through the sample head into the edge of the narrowed deformation zone, which has a typical initial cross-section of 10×10 mm and a length of 12 mm. The maximum speed of each pair of anvils is 350 mm/s,

and the maximum achievable forming force is 196 kN under static loading and 80 kN under dynamic (high speed) loading. When using a hollow head specimen, the realistic rate of controlled cooling with compressed air is up to 15°C/s or up to 1000°C/s in the case of water quenching. The described method of forming in two mutually perpendicular directions as one of the severe plastic deformation (SPD) methods is suitable for obtaining ultra-fine-grained structures of many alloys as well as simulating various high-reduction bulk forming processes – see, e.g. [4-17].

2. Determination of strain value during forming on the MCU MAXStrain II

A significant obstacle to its regular use for simulation became apparent during the commissioning of the MAXStrain II unit (in Ostrava from the end of 2019). The problem lies in the flow of metal out of the nominal deformation zone, even in the case of axial fixation of both sample heads (Fig. 4). From the point of view of calculating the actual equivalent strain e_{eq} (-) in each individual pass, it is then essential that the volume conservation law in the deformation zone can not be applied. Other authors have previously addressed this problem [18,19]. However, their complex calculations based on the tensor or integral calculus do not, in any case, give the possibility of calculating the equivalent strain only based on the published data.

Fig. 4. Detail of thermocouple, deformation zone and adjacent areas of the sample after forming by alternating compressions

Therefore, the primary objective was to develop a simple methodology to calculate the e_{eq} value for the individual passes provided by the MAXStrain II system. The second objective was to use this methodology in a simplified simulation of the temperature-controlled forming and cooling of a long product and evaluate the simulation method's applicability.

A video recording was made of the test process, where a plain carbon steel sample containing 0.17% C – 0.80% Mn – 0.29% Si was formed at a nominal temperature of 950°C for a total of 60 passes with a constant limit setting of opposing anvils. The initial dimensions of the deformation zone were 10×10 mm (cross-section) and 12 mm (length). The compressed dimension after each pass was 6.0 mm, the speed of movement of both anvils was 50 mm/s, and the interpass time was 3.4 s. Images of the sample shape were obtained from the video each time it was spread (see examples in Fig. 5), and their measurement provided information about the value of the partial strains in different directions [20].
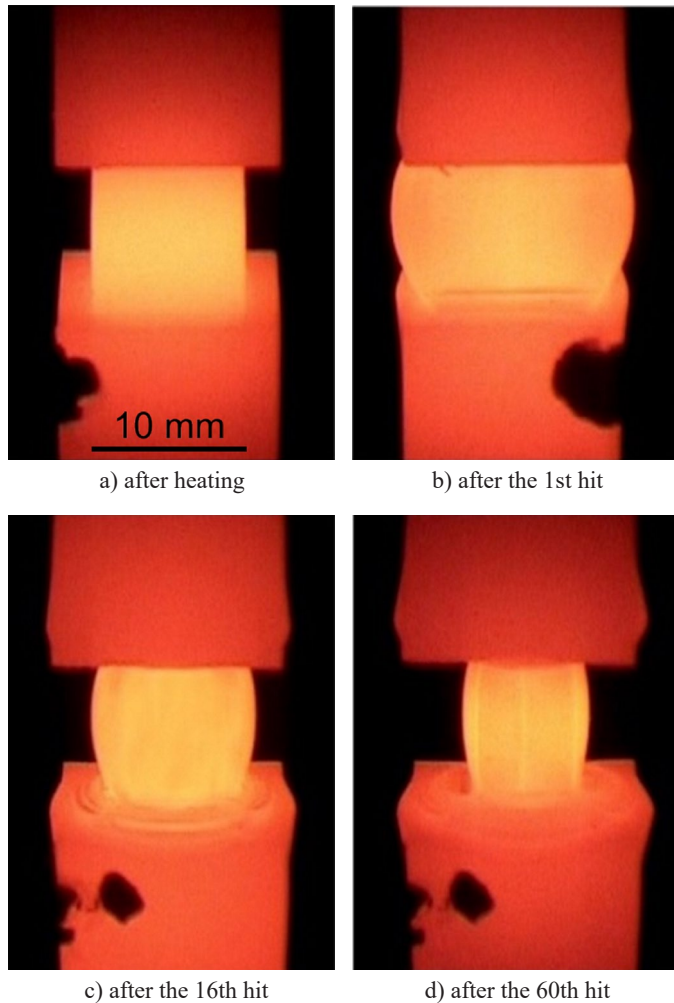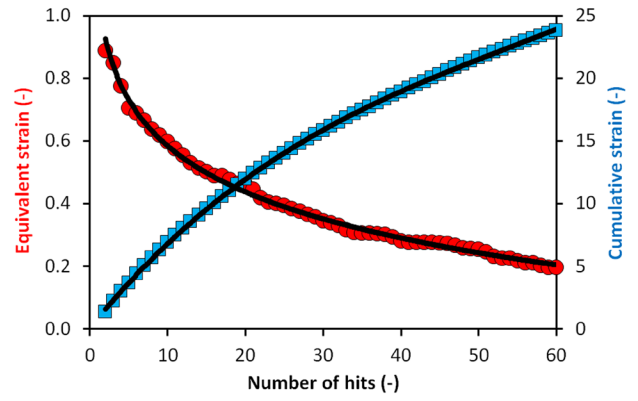

Fig. 6. Strain values depending on the increasing number of hits
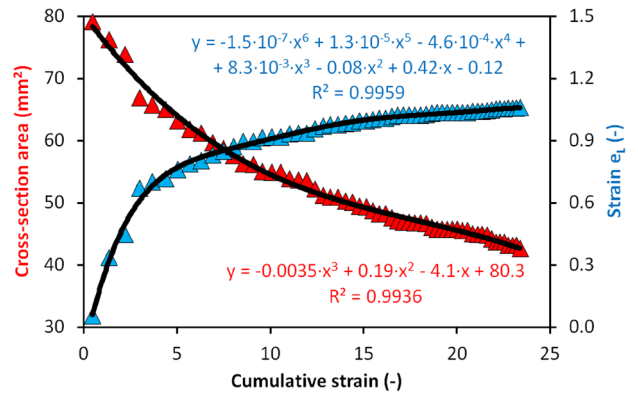
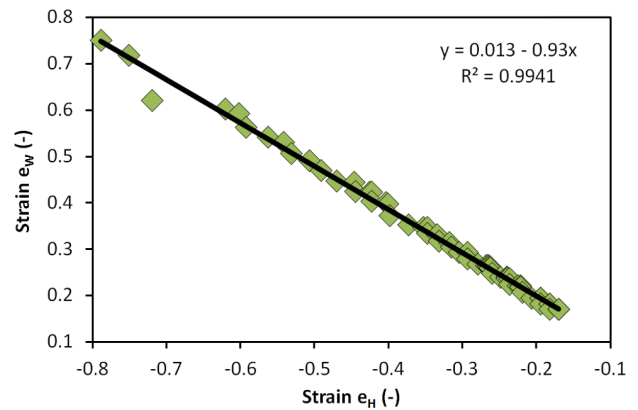Fig. 7. Consequences of changing the cross-section of the sample with increasing strain

a) after heating

b) after the 1st hit

c) after the 16th hit

d) after the 60th hit

Fig. 5. Development of the shape of the sample deformed on the MCU MAXStrain II

Fig. 8. Spreading influenced by the height strain value

The key finding was that the partial equivalent strain e_{eq} decreases with an increasing number of passes and the cumulative strain increases non-linearly (Fig. 6). This is due to the gradual reduction of the sample's cross-section in its deformed part.

It was possible to describe the loss of cross-sectional area and the associated apparent strain in the length direction e_L (-) as a function of the cumulative strain – see the regression relations in Fig. 7. The dependence of the spreading – strain e_W (-) – on the strain in the height direction e_H (-) is practically linear (Fig. 8).

From the strain components in the three mutually perpendicular directions thus determined, the equivalent strain value for the individual passes can then be determined according to the formula

$$e_{eq} = \sqrt{\frac{2}{3} \cdot \left(e_H^2 + e_B^2 + e_L^2 \right)} \tag{1}$$

The quantities e_L, e_W a e_H are with some simplification considered as principal strains. This procedure allows the limits of movement of the anvils to be set for each pass to achieve the desired strains.

3. Experimental

The physical simulation of the continuous rolling of a long product of plain carbon steel containing 0.17 C – 0.80 Mn – 0.29 Si – 0.014 P – 0.026 S – 0.002 Al – 0.0086 N (all in wt.%) used the methodology described above to calculate the value of partial strains. The fictitious rolling was carried out on a mill with four trains, in two temperature variations:

- 1st train – roughing: temperature 1140-1120°C, 4 passes with strain 0.30 at anvil speed 60 mm/s, interpass times 4.5-3.5 s; cooling pause 6 s;
- 2nd train – temperature 1080-1060°C, 6 passes with a strain of 0.25 at an anvil speed of 80 mm/s, interpass times 3.0-2.4 s; cooling pause 6 s;
- 3rd train – temperature 1020-1010°C, 6 passes with a strain of 0.20 at an anvil speed of 100 mm/s, interpass times 1.5-1.0 s; cooling pause 12 s;
- 4th train – finishing: temperature 910-950°C or 850-900°C (with programmed linear temperature increase due to deformation heat), 10 passes with a strain of 0.15 at anvil speed 300 mm/s, interpass times 0.7 s.

The initial samples had hollow heads and a 10×10×12 mm deformation zone. The cumulative equivalent strain of 5.8 corresponds to elongation during the production of a long product of about 330×. The final cooling was carried out after high-temperature rolling at 20°C/s to 900°C and then at 5°C/s to 550°C, and after low-temperature rolling at 20°C/s to 800°C and from there to 550°C at 10°C/s. Fig. 9 compares the shape of the initial sample and the two samples after controlled cooling, exposed at different positions relative to the direction of the last compressive deformation.

Microstructure analysis was performed in the central regions of the sections running transversely through the final thickness of the formed sample. Metallographic samples were etched with 4% Nital solution (a mixture of nitric acid and ethanol) and observed on the Olympus GX51 inverted metallurgical microscope. Structural components were verified using a JEOL JSM-6490LV scanning electron microscope, and secondary electron imaging (SEM SEI) was used for documentation.

Brinell hardness was determined in the central parts of samples after simulations.

4. Results and discussion

4.1. Physical simulations

The plots in Fig. 10 document the time history of both temperature and forming force corresponding to the low temperature variant of the simulation. It is evident that slow hits (with relatively long contact times of cold anvils with the formed sample) lead to variations in the measured temperature. Fig. 11 demonstrates the high accuracy and reproducibility of the experiment in terms of the temporal sequence of the partial passes, as well as the relative increase in forming forces due to the reduction of the finishing temperatures.

It has been shown that compared to uniaxial compression or plane strain compression tests, the applied method is very suitable for simulating forming processes associated with large cumulative strains. The MCU MAXStrain II cooperating with the Gleeble 3800-GTC simulator enables an extreme extent of sample forming to be achieved with relatively uniform structural development in the deformation zone. The weakness of this method is the demanding production of initial samples, the limitations in achieving rapid temperature changes and very
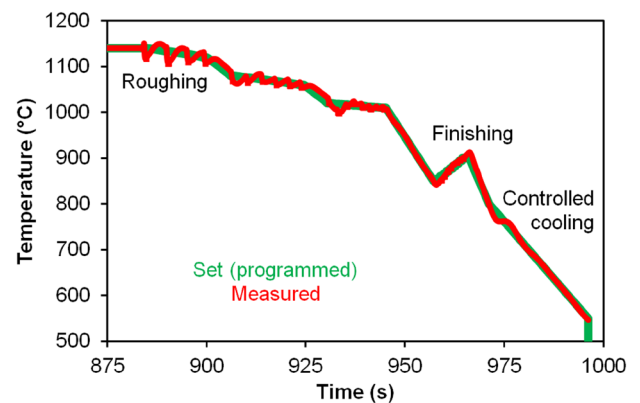
a) temperature
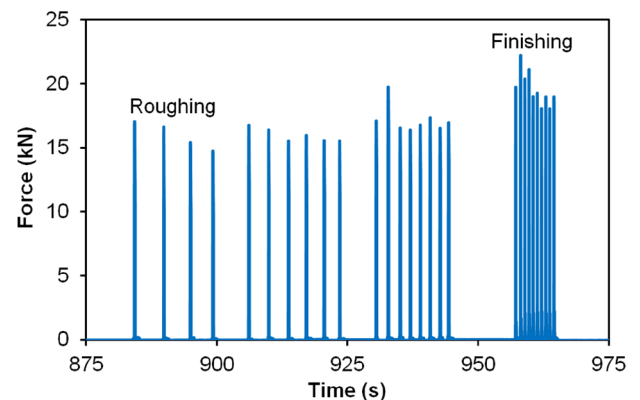
b) forming force

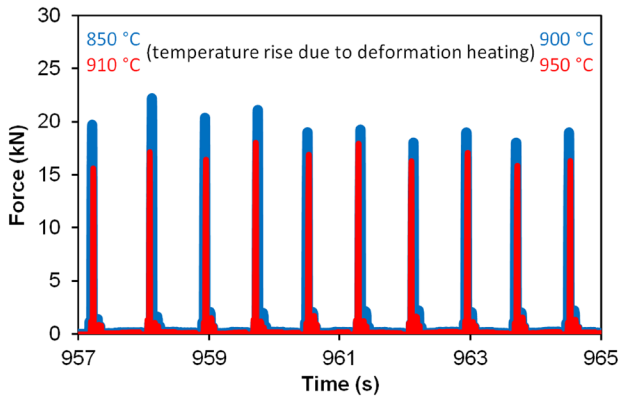Fig. 10. Quantities recorded during the simulation with the low-temperature rolling regime

Fig. 9. Central parts of samples before deformation (above) and after simulations

Fig. 11. Influence of temperature on forming force values in the simulation of finishing (last 10 passes)

Fig. 12. Heterogeneity of microstructure in the middle of the deformation zone

short interpass times, as well as the relatively lower accuracy of temperature control and value of partial strains (e.g., compared to the more commonly used MCU Hydrawedge II). Similar conclusions were reached by the authors of a comparative study [21].

4.2. Optical microscopy

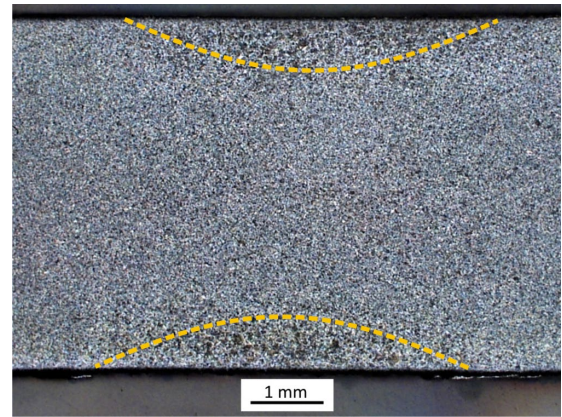As shown by metallographic analyses of the samples after simulations, in the conical subsurface regions, the structure is coarser-grained due to friction between the anvil and the corresponding sample surface (Fig. 12). This is a result of the obvious inhibition of plastic deformation in that regions [22]. However, the heterogeneity of the structure appears less pronounced compared to other samples previously formed by uniaxial compression or PSCT [23,24], which yielded from the alternating action of the anvils in two mutually perpendicular directions.
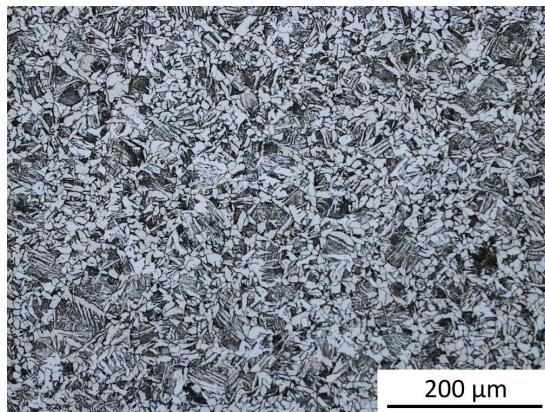
Fig. 13 compares the microstructure of the central regions of the samples after both simulation modes. Using computer
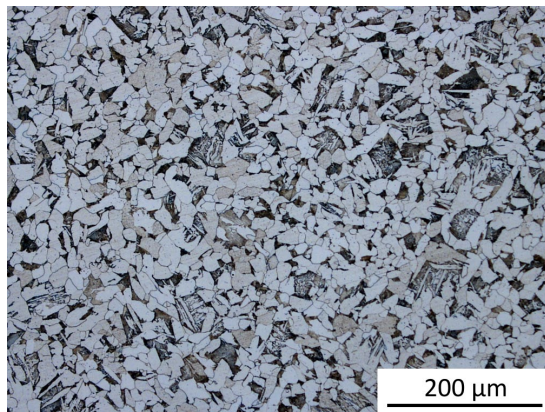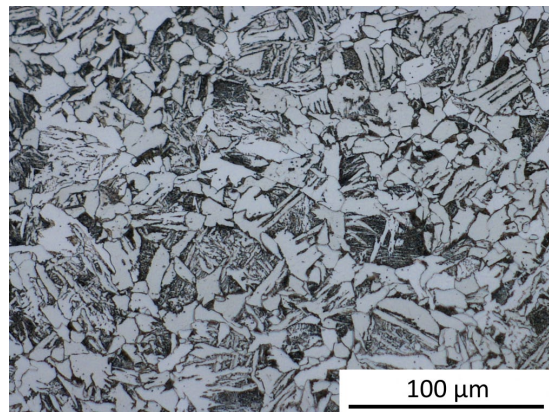

a) high-temperature finishing
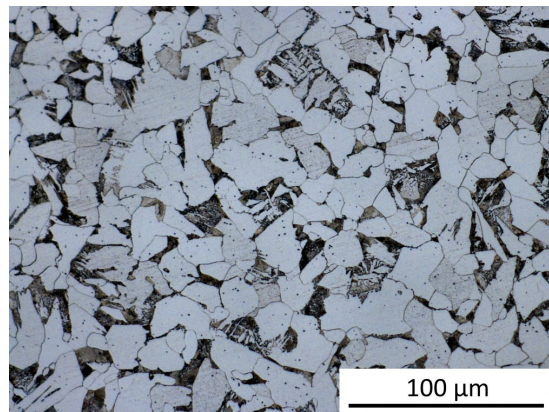
b) high-temperature finishing – close-up view

c) low-temperature finishing

d) low-temperature finishing – close-up view

Fig. 13. Microstructure in the central area of the samples after simulation

image analysis and QuickPHOTO INDUSTRIAL 3.2 software, it was found that increasing the finishing temperature by 50°C and reducing the final cooling rate by half led to a reduction in the occurrence of acicular ferrite and bainite and an increase in the mean grain size of proeutectoid ferrite from 8.0 μm to 14.1 μm. This was reflected in a decrease in hardness from 190 HBW to 162 HBW.

4.3. Electron microscopy

Some details obtained by SEM are presented in Fig. 14. In the case of high-temperature finishing and slower cooling, the structure is predominantly ferritic-perlitic, consisting of polyhedral grains of proeutectoid ferrite (PF) with a minor lot of pearlite (P). Minor areas of acicular ferrite (AF) occur within the original austenitic grains, with pearlite predominating among the needles and only trace amounts of bainite (B). In the case of low temperature rolling and more rapid cooling, polyhedral ferrite grains are located in the area of the boundaries of the original austenitic grains (allotriomorphic ferrite) together with perlite regions; within the grains, acicular ferrite occurs together with bainite and perlite is present only in trace amounts.

5. Conclusions

- Two temperature variants of continuous rolling and controlled cooling simulations were performed using the MAXStrain II system and a newly developed methodology for calculating the equivalent strain value during alternating forming in two directions. The described calculation procedure is relatively simple, manageable in a common spreadsheet, but probably not completely universal. It should be refined for other types of formed samples (in shape or dimensions) and for fundamentally different types of investigated material tests with varying deformation temperatures – for example, aluminium alloys.
- The performed simulation experiments confirmed the fundamental influence of the rolling temperature and, in particular, the cooling conditions on the structural and mechanical properties even in the case of conventional plain carbon steel with 0.17% C. Increasing the finishing temperature from 900°C to 950°C and decreasing the final cooling rate from 10°C/s to 5°C/s led to a decrease in the content of both acicular ferrite and bainite and to an increase in the mean grain size of proeutectoid ferrite from about 8 μm to 14 μm. This resulted in a decrease in hardness by 15%.
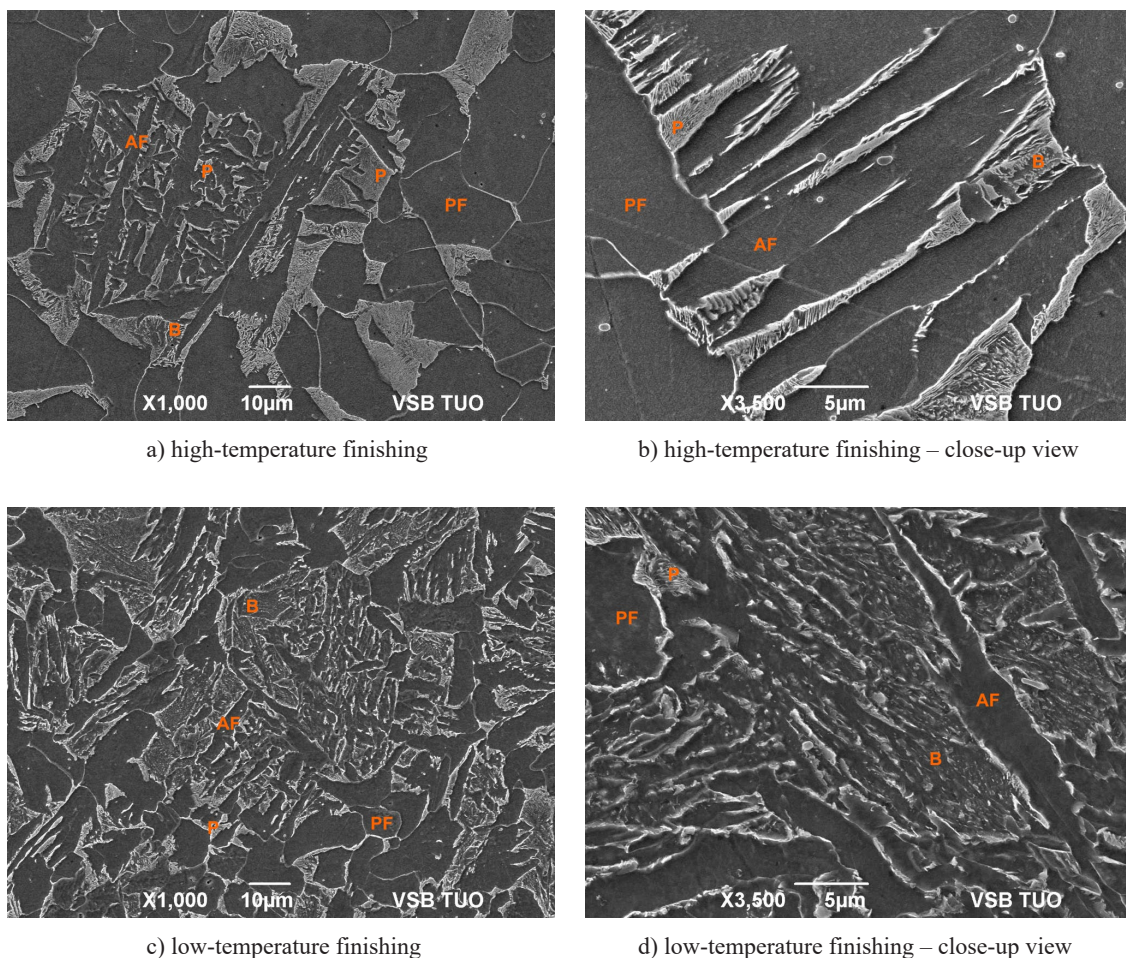

a) high-temperature finishing

b) high-temperature finishing – close-up view

c) low-temperature finishing

d) low-temperature finishing – close-up view

Fig. 14. Microstructure in the central regions of the original austenitic grains (SEM)

Acknowledgements

REFERENCES

[1] https://www.gleeble-tech.com/gleebledocs/g5/desc_and_specs/index.html#, accessed: 02.05.2022

[2] I. Schindler, P. Kawulok, P. Opěla, R. Kawulok, K. Konečná, M. Konderla, S. Rusz, R. Fabík, J. Němec, Hutnické listy **75** (3-4), 17-22 (2022).

[3] P. Kawulok, R. Kawulok, I. Schindler, S. Rusz, J. Kliber, P. Unucka, K.M. Čmiel, Metalurgija **53** (3), 299-302 (2014).

[4] S.T. Mandziej, M. Ruggeri, Materials Science Forum **762**, 55-61 (2013).
DOI: https://doi.org/10.4028/www.scientific.net/MSF.762.55

[5] W.C. Chen, D. Ferguson, H.S. Ferguson, R.S. Mishra, Materials Science Forum **357-359**, 425-430 (2001).

[6] R. Kuziak, W. Zalecki, S. Weglarczyk, Solid State Phenomena **101-102**, 43-48 (2005).
DOI: https://doi.org/10.4028/www.scientific.net/SSP.101-102.43

[7] J. Majta, K. Muszka, Materials Science and Engineering A **464** (1-2), 186-191 (2007).
DOI: https://doi.org/10.1016/j.msea.2007.01.135

[8] H. Petryk, S. Stupkiewicz, R. Kuziak, Journal of Materials Processing Technology **204** (1-3), 255-263 (2008).
DOI: https://doi.org/10.1016/j.jmatprotec.2007.11.068

[9] S. Kleber, M. Hafok, Materials Science Forum **638-642**, 2998-3003 (2010).
DOI: https://doi.org/10.4028/www.scientific.net/MSF.638-642.2998

[10] J. Bystrzycki, A. Fraczkiewicz, R. Lyszkowski, M. Mondon, Z. Pakiela, Intermetallics **18**, 1338-1343 (2010).
DOI: https://doi.org/10.1016/j.intermet.2010.01.014

[11] K. Rodak, K. Radwański, R.M. Molak, Solid State Phenomena **176**, 21-28 (2011).
DOI: https://doi.org/10.4028/www.scientific.net/SSP.176.21

[12] Y. Wu, H. Yan, J. Chen, Y. Du, S. Zhu, B. Su, Materials Science & Engineering **556**, 164-169 (2012).
DOI: https://doi.org/10.1016/j.msea.2012.06.074

[13] P. Bereczki, V. Szombathelyi, G. Krállics, IOP Conference Series: Materials Science and Engineering **63**, (2014).
DOI: https://doi.org/10.1088/1757-899X/63/1/012140.

[14] V. Komarov, I. Khmelevskaya, R. Karelin, S. Prokoshkin, M. Zaripova, M. Isaenkova, G. Korpala, R. Kawalla, Journal of Alloys and Compounds **797**, 842-848 (2019).
DOI: https://doi.org/10.1016/j.jallcom.2019.05.127

[15] M. Wojtaszek, G. Korpala, T. Śleboda, K. Zyguła, U. Prahl, Metallurgical and Materials Transactions A **51**, 5790-5805 (2020).
DOI: https://doi.org/10.1007/s11661-020-05942-7

[16] M.S. Jalme, C. Desrayaud, J. Favre, D. Fabregue, S. Dancette, C. Schuman, J. Lacomte, E. Archaud, C. Dumont, Materials Science Forum **1016**, 1211-2017 (2021).
DOI: https://doi.org/10.4028/www.scientific.net/MSF.1016.1211

[17] J. B. Renkó, G. Krállics, Materials Today: Proceedings **45**, 4100-4104 (2021).
DOI: https://doi.org/0.1016/j.matpr.2020.11.329

[18] H. Petryk, S. Stupkiewicz, Materials Science and Engineering A **444**, 214-219 (2007).
DOI: https://doi.org/10.1016/j.msea.2006.08.076

[19] P. Bereczki, V. Szombathelyi, G. Krállics, International Journal of Mechanical Sciences **84**, 182-188 (2014).
DOI: https://doi.org/10.1016/j.ijmecsci.2014.04.025

[20] H. Navrátil, I. Schindler, P. Kawulok, P. Opěla, R. Kawulok, in: 31st International Conference on Metallurgy and Materials METAL 2022, TANGER s.r.o., 302-307 (2022).
DOI: https://doi.org/10.37904/metal.2022.4464

[21] Yu.A. Bezobrazov, N.G. Kolbasnikov, A.A. Naumov, Steel in Translation **44**, 71-79 (2014).
DOI: https://doi.org/10.3103/S0967091214010057

[22] Y.C. Lin, M.S. Chen, J. Zhong, Computational Materials Science **43** (4), 1117-1122 (2008).
DOI: https://doi.org/10.1016/j.commatsci.2008.03.010

[23] P. Kawulok, A. Mertová, I. Schindler, R. Kawulok, S. Rusz, P. Opěla, J. Macháček, G. Urbanová, K. Brada, R. Kafka, Kovárenství **57**, 23-28 (2016).

[24] I. Schindler, P. Kawulok, S. Rusz, R. Kawulok, P. Šimeček, Z. Vašek, Hutnické listy **66** (4), 61-66 (2013).